






Article

A Hierarchical Multi-Stage Coordination of Inverters for Voltage Control in Active Distribution Networks with a μ PMU-PDC

Ali Zafari ¹, Ameen Gargoom ^{1,*}, Nasser Hosseinzadeh ¹, Shama Islam ¹, Md Enamul Haque ¹,
Mohammad Taufiqul Arif ¹ and Mohamed Abdelrazek ²

¹ Center for Smart Power and Energy (cSPER), School of Engineering, Deakin University, Geelong 3216, Australia

² School of Information Technology, Deakin University, Melbourne 3125, Australia

* Correspondence: a.gargoom@deakin.edu.au

Abstract: This paper proposes a hierarchical multi-stage approach based on a distributed level phasor measurement unit (μ PMU) at local controllers and a phasor data concentrator (PDC) at the central control unit to restore system voltage when it exceeds the limits recommended by the IEEE 1547-2018 standard. The proposed algorithm does not need an accurate system model or employ optimization solutions. Therefore, it has less implementation complexity and would be popular among distribution network service providers (DNSPs) and distribution network operators (DNOs) as it does not suffer from cost and computational complexity limitations. A PMU-PDC-based communication platform has been developed as a more efficient alternative to the supervisory control and data acquisition (SCADA) system, and provides superior characteristics, including a higher sample rate, higher data resolutions, and faster communication. The proposed coordinated algorithm aims to postpone power generation curtailment in distributed energy resources (DERs) with overvoltage problems (local DERs) by incorporating all the DERs that are not subjected to voltage violation (remote DERs) by absorbing their maximum reactive power capacity. If the system voltage has not recovered after absorbing all of the reactive power capacity of all the DERs, a reduced active power curtailment proposed by the algorithm is then applied to the system to control the voltage. The proposed strategy has been simulated in MATLAB and applied to IEEE 13-bus and IEEE 33-bus radial distribution benchmark systems to validate the performance of the system, in terms of its ability to coordinate voltage control and the accuracy of the PMU-PDC-based communication interface.

Keywords: voltage regulation; active distribution networks; phasor measurement unit (PMU); phasor data concentrator (PDC)



Citation: Zafari, A.; Gargoom, A.; Hosseinzadeh, N.; Islam, S.; Haque, M.E.; Arif, M.T.; Abdelrazek, M. A Hierarchical Multi-Stage Coordination of Inverters for Voltage Control in Active Distribution Networks with a μ PMU-PDC. *Energies* **2023**, *16*, 4650. <https://doi.org/10.3390/en16124650>

Academic Editor: Dinko Vukadinović

Received: 27 April 2023

Revised: 6 June 2023

Accepted: 7 June 2023

Published: 12 June 2023



Copyright: © 2023 by the authors. Licensee MDPI, Basel, Switzerland. This article is an open access article distributed under the terms and conditions of the Creative Commons Attribution (CC BY) license (<https://creativecommons.org/licenses/by/4.0/>).

1. Introduction

Electrical distribution networks are undergoing a paradigm shift with the rapid deployment of distribution energy resources (DERs), enabling end-users to participate as prosumers in active distribution networks (ADNs). However, with the large integration of DERs and the consequent reverse power flow, voltage regulation has emerged as a major concern for distribution network operators (DNOs), due to voltage violations occurring outside the permitted range (e.g., $0.95 \text{ pu} < v_{bus} < 1.05 \text{ pu}$, recommended by ANSIC84.1-2016 [1] and IEEE 1547-2018 [2] standards). In response, various functions have been integrated into the inverters of DERs, enabling them to function as smart inverters (SIs) and ensure acceptable power quality and reliability of supply [3]. However, these functions typically operate based on local information/measurements and respond individually. To achieve more efficient voltage regulation in ADNs, coordination among the inverters is necessary to provide enhanced visibility and better control over the voltage profile across the distribution network.

However, to fully realize the benefits of coordinated voltage regulation, two technical challenges must be taken into consideration. The first is the design and implementation of an effective control algorithm that can coordinate the operation of smart inverters. The second is the development of a robust communication system that can reliably transmit information between the local controllers and a central control unit.

In the area of control algorithms, there have been several research studies on the coordinated operation of DERs with other voltage regulation devices, such as on-load tap changers (OLTC) and capacitor banks, to enhance the flexibility of a voltage regulation system [4]. One such approach is a two-stage online algorithm proposed in [5], which employs DERs as a complementary solution to control the voltage violation problem. In the first stage, OLTCs are scheduled using a multi-time-step optimization problem, and in the second stage, DERs are incorporated to control the voltage violation problem. The authors of [6] proposed an optimal coordinated approach for OLTC and DERs supplied by battery energy storage systems (BESSs) to minimize system voltage violations, with a focus on minimizing OLTC tap switching and reducing BESS usage. In [7], a model predictive control (MPC)-based method was suggested to optimally coordinate the generation in DERs, power of the BESS, and OLTC tap position to maintain the voltage within permissible ranges. The approach proposed in [8] is a coordinated strategy based on the alternating direction method of multipliers (ADMM) and optimal control to regulate the system voltage, which is shown to achieve a 20% improvement in voltage regulation while reducing the number of OLTC taps. The authors of [9] introduced a control approach based on the micro/recursive genetic algorithm optimization method to coordinate the performance of OLTC, the capacitor bank, and DER in the ADN, aiming to achieve optimum tap changing and minimum power losses. In [10], a coordinated control method based on a multi-agent system was proposed to minimize either the voltage violation or stress on passive voltage regulator devices.

In addition, various coordination approaches have been investigated in the literature to improve voltage regulation performance in ADNs. To minimize voltage deviations or power losses, a multi-objective hierarchical Volt/Var control (VVC) strategy was introduced in [11], which optimizes reactive power set points and p-droop characteristics in both local and central control units. Similarly, in [12], a coordinated voltage regulation algorithm was proposed that utilizes optimal reactive power from photovoltaic (PV)-based DERs and optimal charging/discharging power from battery energy storage systems (BESSs) for reactive and active power control. To allocate the optimal reactive power set point in DERs, a feedback-based leader–follower consensus algorithm was used to formulate the voltage regulation problem as an optimization problem in [13]. The authors of [14] proposed a globally optimum solution to control the system through coordinated active and reactive power exchanges between the DERs and distribution networks. Additionally, to minimize the incorporation of the main grid capacity and to specify the optimum operating point in DERs, a model-free coordinated strategy based on an extremum-seeking control approach was provided in [15].

Overall, these studies highlight the importance of coordinated voltage regulation in ADNs, which can lead to a more efficient control performance and better utilization of DERs. However, through a comprehensive review of the existing literature, the authors of this study have noticed that most current approaches to control and optimize power distribution systems require accurate models and complex optimization techniques. While these methods are theoretically sound, they can be cost-prohibitive and computationally burdensome for distribution network supply providers and distribution network operators (DNSPs and DNOs). To address these limitations, this paper proposes a novel algorithm that eliminates the need for complex optimization solutions and accurate system models. By doing so, the algorithm significantly reduces both the mathematical burden and overall cost, making it a more practical solution for DNSPs and DNOs.

In addition to control algorithms, communication systems play a critical role in voltage regulation in ADNs. Most utilities have traditionally used the supervisory control

and data acquisition system (SCADA) in the distribution networks for monitoring and control purposes [16]. The SCADA system captures unsynchronized voltage and current magnitudes, as well as active and reactive power readings from conventional measurement devices [17,18]. However, the low resolution of data and the inability to record the dynamic performance of the network are considered to be significant limitations of the SCADA-based communication system [19]. These limitations can lead to inaccurate system analysis and control, which can result in power quality issues, voltage fluctuations, and other operational problems.

On the other hand, the deployment of phasor measurement units (PMUs) that report to phasor data concentrators (PDCs), with a high time-stamp resolution, can provide system visibility enhancement much greater than that provided by SCADA. A distributed-level phasor measurement unit (D-PMU or μ PMU) has been developed as a more effective alternative to the SCADA system in the distribution network and provides superior characteristics, including a higher sample rate (maximum 100 and 120 frames per second for a 50 Hz and 60 Hz nominal system frequency, respectively, recommended by IEEE C37.118.1 standard [20]), higher data resolutions, fast communication, accurate synchronization achieved by utilizing global positioning system (GPS) antenna, and the capability to support a large number of devices [21,22]. Several research studies, such as [23–26], have reported on μ PMU application in distribution networks, in terms of monitoring, diagnostics, and control systems. In [27] and [25], μ PMU was represented as a system that could be incorporated into the planning and modeling of a system with a high penetration of DERs, as well as reconfiguration, power restoration, and island operation.

To ensure the effective coordination among the DERs in ADNs, a communication system based on μ PMUs and phasor data concentrators (PDCs) has emerged as a promising solution. The μ PMUs provide high-resolution, time-synchronized measurements of the system's voltage and current phasors, while the PDCs act as centralized data aggregators that collect and process the μ PMU data. The communication protocol used between the μ PMUs and PDCs is specified in the IEEE Std. C37.118.2 [28]. By leveraging this robust communication interface, the coordinated performance of DERs can be improved to enhance the overall stability and efficiency of the ADN.

Although there have been some papers published on the coordinated performance of DERs in ADN using μ PMU and PDC communication, the existing literature remains limited. This underscores the need to further develop and refine coordinated strategies using a μ PMU/PDC communication platform to fully realize the potential benefits of DERs in ADN.

This paper, therefore, presents a hierarchical multi-stage algorithm for voltage regulation in distribution networks with DERs. The algorithm aims to restore the system voltage within the limits recommended by IEEE 1547-2018 while alleviating power curtailments in case of over voltages. The proposed algorithm comprises four stages, where DERs are coordinated to regulate the system voltage. In the first stage, all DERs act independently to restore the voltage at the connection point through reactive power exchange with the network. In the next three stages, the central control unit and the local controllers communicate with each other to coordinate DER functions and to make decisions to minimize power generation curtailment in the system. To ensure the feasibility of the proposed algorithm, a communication interface based on phasor measurement units (PMUs) in local controllers and a phasor data concentrator (PDC) in the central control unit is proposed and tested. It is worth noting that while the use of μ PMUs is proposed in this paper to facilitate the coordination of DERs for voltage regulation, these devices can also be deployed to improve the visibility of the distribution network, which can benefit a range of other applications beyond voltage regulation.

The main benefits of the proposed algorithm are:

- The proposed algorithm does not require an optimization solution or an accurate system model, which reduces the mathematical burden and the overall cost considerably.

- The algorithm effectively postpones the PV power generation curtailment in DERs by incorporating all the DERs in absorbing reactive power using a coordinated strategy predicted in Stage II of the algorithm.
- The algorithm manages power generation curtailment in each DER by monitoring the overall curtailment index (CI) as well as the curtailment distribution (CD) in the entire system and making decisions to improve these indices in Stage III of the algorithm.
- The algorithm ensures the maximum capacity utilization of all the DERs for voltage restoration and avoids other solutions by considering the least power generation curtailment in Stage IV of the algorithm.

Overall, these features make the proposed algorithm a cost-effective and efficient solution for DNSPs and DNOs, offering improved voltage control and reduced power generation curtailment in DERs.

In addition, a mathematical assessment of the impact of remote distributed energy resources (DERs) on the voltage control of local DERs, particularly when subjected to voltage violations, is presented in the paper. This assessment is critical to ensure the overall stability and reliability of the proposed algorithm. To validate the effectiveness of this approach, rigorous simulation case studies are conducted using the IEEE 13-bus radial distribution benchmark feeder [29]. The results demonstrate the robustness and scalability of the algorithm in managing voltage violations and optimizing the utilization of DERs.

The rest of the paper is organized as follows. Section 2 provides a brief overview of the proposed algorithm for the coordination of voltage regulation devices. Section 3 presents the details of the WSN-based communication system used for monitoring and control. Section 4 presents the simulation results to demonstrate the effectiveness of the proposed algorithm and communication system. Finally, conclusions are drawn in Section 5.

2. The Proposed Voltage Regulation Strategy

This section outlines the proposed strategy for regulating the bus voltages, which is divided into two subsections. The first subsection introduces the general framework of the proposed algorithm, while the second subsection provides a detailed explanation of the proposed coordination algorithm using a conceptual flowchart.

2.1. The General Framework of the Proposed Algorithm

The framework of the proposed algorithm consists of two main parts: a local control and a central control (PDC), as shown in Figure 1. The local control assigns the reference (set) values of the active and reactive power (p_{ref}^i and q_{ref}^i) to the i th DER's PQ controller using the related p-droop and q-droop functions, respectively. These set values are updated as needed using the approach explained in the next subsection.

The central control modifies the parameters for the p- and q-droop functions in the PDC by analyzing the data received from all the PMUs located in the covered area of the distribution network. This is accomplished by executing the proposed coordinated strategy described in the next subsection. The proposed algorithm involves adjusting the dead-band voltages ($v_D^{p,i}$, $v_D^{q,i}$) and inflection points ($v_{inf}^{p,i}$, $v_{inf}^{q,i}$) in both the p- and q-droop functions related to the i th DER, as denoted in Figure 2. These control variables are used to fine-tune the setting points for the local controllers. The maximum exchangeable reactive power in the i th DER (Q_{max}^i), as a saturated level denoted in Figure 2, is also assigned according to the permitted ranges recommended by the IEEE 1547-2018 standard, as depicted in Figure 3, by considering the available active power generation (P_{ava}^i) in each DER.

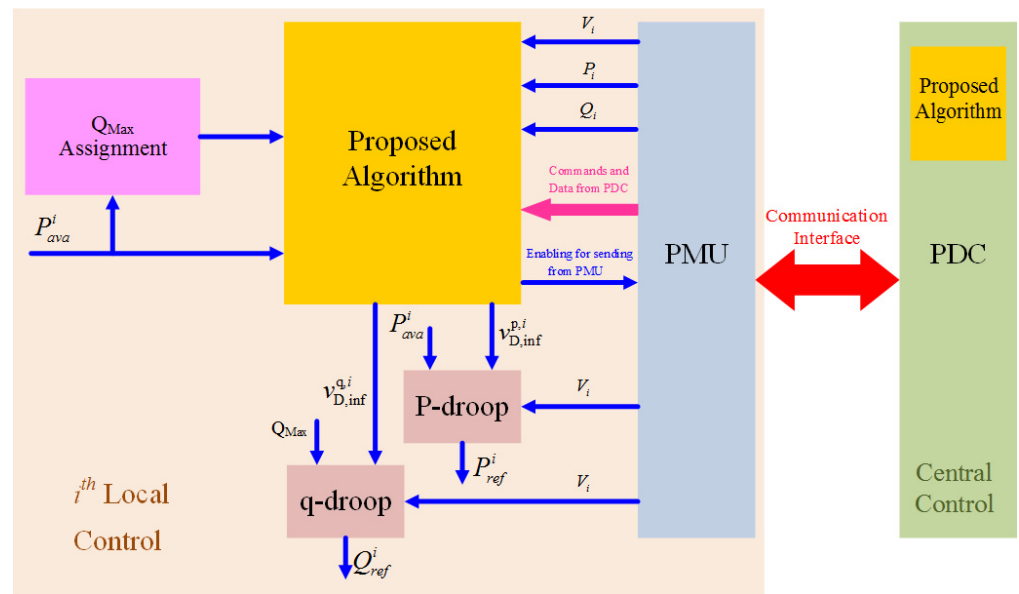


Figure 1. The general framework of the proposed control strategy.

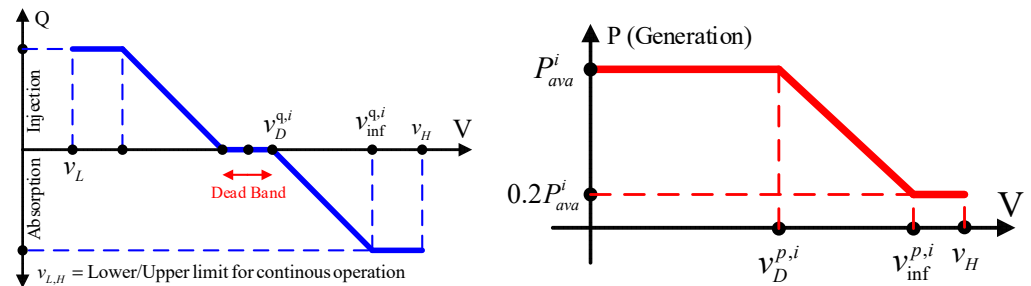


Figure 2. p-droop and q-droop functions associated with the i th DER.

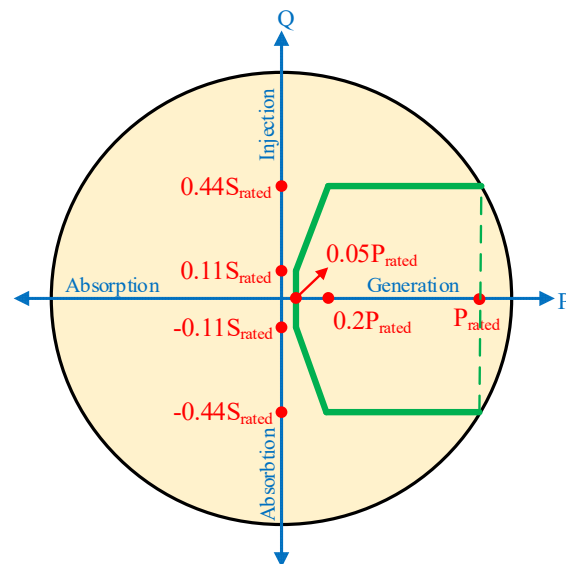


Figure 3. Permitted ranges for exchangeable reactive power recommended by the IEEE 1547-2018 standard (the green solid lines represent the boundaries for the reactive power limit).

While the measurements communicated to the PDC from the DERs include the magnitude (rms) values and phase angles of both the voltage and current at the buses, only the rms value of the voltage is used. The modified droop parameters calculated in the

local or central controllers are assigned to the droop functions, as elaborated in the following subsection. The communication network for the proposed algorithm is discussed in Section 3.

2.2. DERs Coordination Algorithm

To maintain the system voltage within acceptable limits and enhance power generation from the DERs, a four-stage coordination algorithm is proposed. This algorithm enables local and central control units to make measurements and decisions based on voltage violations, with the ultimate goal of regulating voltage while enhancing DER power generation. The algorithm is illustrated in a conceptual flowchart shown in Figure 4, where the measurements and decisions are performed by both local and central control units denoted by L and C, respectively.

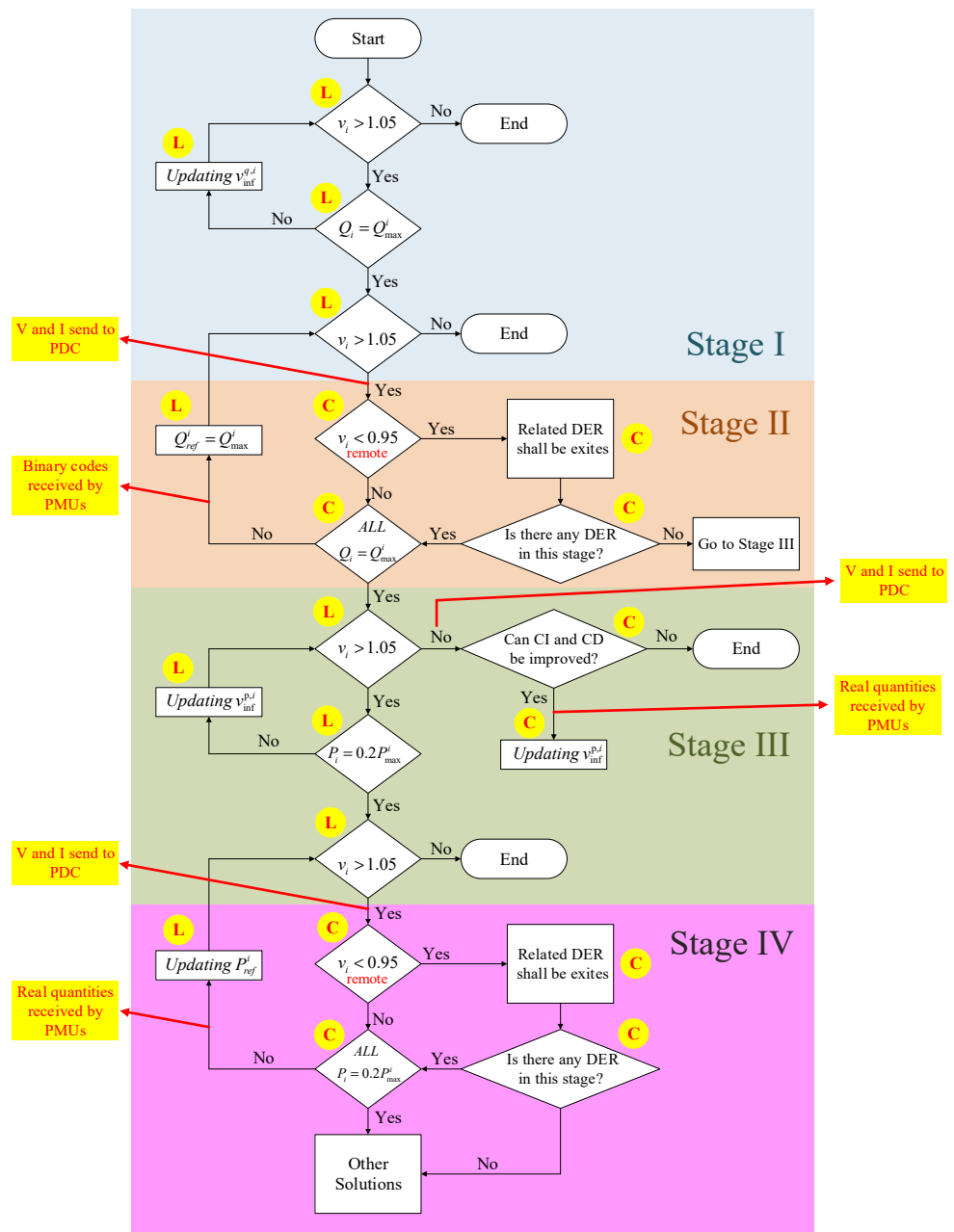


Figure 4. A conceptual flowchart for the proposed control algorithm.

In Stage I, DERs that experience exceeded voltage limits independently regulate the voltage at the point of connection (POC) by absorbing reactive power. The dead-band voltage ($v_D^{q,i}$) is maintained constant at 1.05 pu, which is the maximum permitted value recommended by the ANSIC84.1-2016 and IEEE 1547-2018 standards. The inflection points in the q-droop functions ($v_{inf}^{q,i}$) are updated through interpolation, with a starting value of 1.1 pu as an upper permitted voltage in a continuous range. If local controllers cannot regulate the system voltage in Stage I (when the reactive power of the DER reaches Q_{max}^i), the DERs that are not experiencing voltage violations are designated as remote DERs, and their specifications are sent to the PDC.

In Stage II, if the local controllers cannot regulate the system voltage through the reactive power exchange in Stage I, remote DERs are enlisted in the PDC to assist in voltage recovery. All the q-droops of the remote DERs are set to absorb the maximum capacity of reactive power (Q_{max}^i). However, as the voltage at the remote DERs starts to decrease due to reactive power absorption, it is necessary to ensure that their voltage does not drop below 0.95 pu. Therefore, a complementary loop is added to Stage II to check the lower limit of the voltage after checking the upper limit, as shown in Figure 4. If the voltage drops below the lower limit, the relevant DER is excluded from the central controller and returned to the local control unit to regulate the voltage. This ensures that only DERs with voltages above the lower limit are allowed to participate in voltage recovery. One of the advantages of this stage is that it postpones power curtailment by using the maximum capacity of the reactive power of all the DERs for regulating the system voltage.

In the event that the voltage remains unregulated at the end of Stage II, the algorithm proceeds to Stage III, in which any DER experiencing high voltage levels enters the p-droop mode. This stage involves the local controls of the DERs for curtailing power generation at the POC to regulate the voltage in a timely and effective manner. To achieve this, the active power reference values are updated continuously by adjusting the inflection points ($v_{inf}^{p,i}$) in the p-droop function. Starting with a value of 1.1 pu, the value of $v_{inf}^{p,i}$ is reduced in steps, while maintaining the dead-band voltage ($v_D^{p,i}$) constant at 1.05 pu. Figure 5 provides a visual representation of the p-droop function for various values of $v_{inf}^{p,i}$.

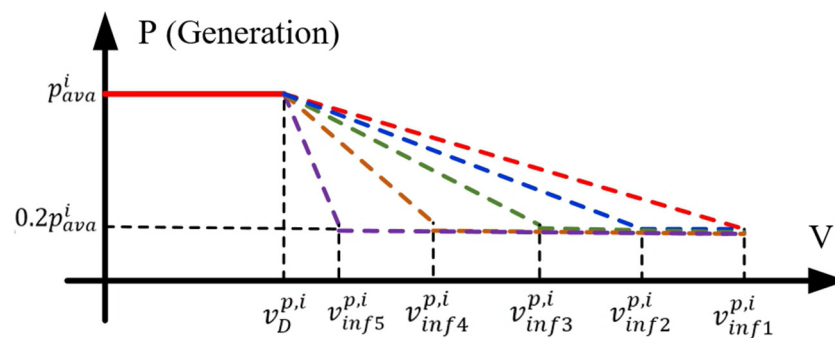


Figure 5. The p-droop function for different values of $v_{inf}^{p,i}$.

To enhance the efficiency of the system in terms of active power curtailment, Stage III includes an evaluation of the curtailment index (CI) and curtailment dispatch (CD) provided by (1) and (2), respectively. Note that lower values for CI and CD indicate better system conditions. To this end, an additional condition has been added to the flowchart after voltage recovery, as shown in Figure 4. In this section, the central controller evaluates other possibilities for curtailment to identify the most efficient option in terms of CI and CD. If a more efficient alternative is detected, a modified $v_{inf}^{p,i}$ value is assigned and sent to the local controllers before ending the flowchart in Stage III. By performing this evaluation,

the system can achieve a lower active power curtailment, leading to improved system performance and stability.

$$CI = \frac{\text{curtailed power}}{\text{available power}} = \frac{\sum_i P_{cur}^i}{\sum_i P_{ava}^i} \quad (1)$$

$$CD = \frac{CI}{N} \quad (2)$$

where n is the number of DERs in the covered area of the distribution network of the feeder.

In the fourth stage, if the voltage is still not regulated, the DERs that are not affected by the voltage violation are designated as remote DERs for power curtailment to lower the voltage in the local DERs that are still experiencing high voltage levels. To limit the amount of curtailment required, it is advisable to gradually decrease the power generation of the remote DERs by adjusting the active power reference in multiple stages. This involves using several reference active power values (p_{ref}^i) instead of starting at the minimum value ($0.2p_{ava}^i$, as per the standard). In this way, the curtailment is reduced, and the system experiences less power interruptions. The number of steps for remote curtailment per DER should be limited (up to a maximum of four steps in this study).

2.3. Assessment of the Impact of Remote DERs on Voltage Control in Local DERs

Since the proposed algorithm is based on the coordinated performance of DERs in system voltage control, it would be much more beneficial if the impact of the remote DERs on the voltage regulation at the local bus was mathematically formulated to increase the technical support of the proposed control strategy. To this end, the IEEE 13-bus radial distribution feeder (IEEE-13 feeder) was simplified, as illustrated in Figure 6. In this system, all the left side loads at B1 are modeled as P_{L1} and Q_{L1} . In addition, the left side loads at B2 are represented as PV in the active and reactive injection modes to model a voltage increase at B2. Three DERs are assumed to be installed at B2 as a local bus, and at B3 and B5 as remote buses. It is assumed that the operating condition is in Stage II of the algorithm and the remote DERs are incorporated to regulate the voltage at the local bus through only reactive power absorption.

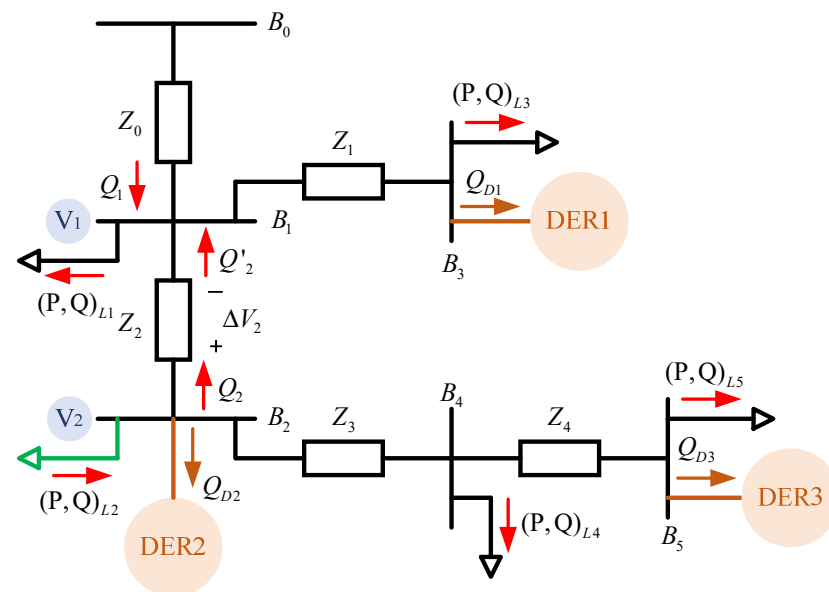


Figure 6. A simplified model of the IEEE 13-bus radial distribution feeder (IEEE-13 feeder).

By considering ΔV_2 as a voltage drop across Z_2 and ignoring the impact of the phase difference between V_1 and V_2 on voltage regulation, the relationship between the voltage at B1 and B2 can be explained as (3).

$$V_2 = V_1 + \Delta V_2 \quad , \quad \Delta V_2 = \sqrt{\frac{Z_2^2}{X_2}(Q_2 - Q'_2)} \tag{3}$$

where Q_2 and Q'_2 are the sending reactive power from B_2 and the receiving reactive power at bus B_1 , respectively, which can be expressed by (4) and (5), respectively.

$$Q_2 = Q_{L2} - Q_{L4} - Q_{L5} - Q_{D2} - Q_{D3} \tag{4}$$

$$Q'_2 = Q_{L1} + Q_{L3} - Q_1 + Q_{D1} \tag{5}$$

Q_{D1} , Q_{D2} , and Q_{D3} represent the reactive power absorbed by DER1, DER2, and DER3, respectively. The reactive power exchanged through all the loads can be assumed to be constant values during voltage regulation intervals. Moreover, since the reactive power absorbed by the local DER (Q_{D2} in this case) is set at the maximum value (Q_{D2}^{max}) in Stage II, it can be assumed to be a constant value as well. Therefore, constants k_1 and k_2 can be defined as $k_1 = Q_{L2} - Q_{L4} - Q_{L5} - Q_{D2}$ and $k_2 = Q_{L1} + Q_{L3}$ and (3) is rewritten as (6).

$$V_2 = V_1 + \sqrt{\frac{Z_3^2}{X_3}(k_1 - k_2 + Q_1 - Q_{D1} - Q_{D3})} \tag{6}$$

By considering $k_3 = k_1 - k_2$, and assuming 1.05 pu as the maximum permitted voltage in an overvoltage area as recommended by IEEE1547, (6) is expressed as an inequity provided by (7).

$$V_2 = V_1 + \sqrt{\frac{Z_3^2}{X_3}(k_3 + Q_1 - Q_{D1} - Q_{D3})} < 1.05 \tag{7}$$

Figure 7 presents a 3D plot of (7) for five different values of V_1 . The surface plots show the relationship between the absorbed reactive power by DER1 and DER3, as well as the reactive power available at bus B_1 (Q_1). The plots were generated in response to a voltage rise of 1.05 pu at bus B_2 (the local bus) to identify the layers of the operating points. The operating points above the surface indicate a voltage level greater than 1.05 pu, while the operating points below the surface represent a voltage level less than 1.05 pu at B_2 .

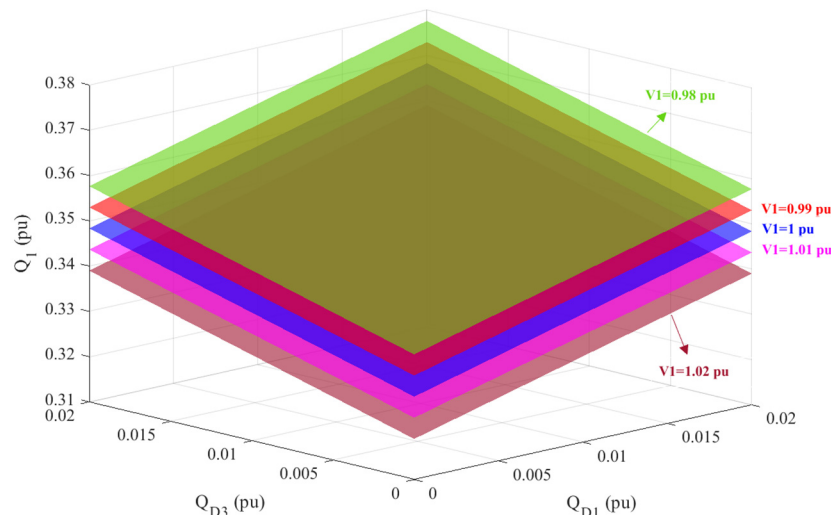


Figure 7. A 3D plot of (7) for five different values of V_1 .

To validate the analysis, the system shown in Figure 6 was simulated using MATLAB (R2022a), and the voltage at bus B2 was measured for five different scenarios, including no compensation, compensation using only DER2, and compensation by deploying remote DERs with operating points determined by the values across/over/under the surface, as depicted in Figure 7. As seen in Figure 8, the voltage at B₂ was found to increase to 1.067 pu in the overvoltage case and decrease to 1.054 pu in Stage I. In Stage II, the remote DERs (DER1 and DER3) were integrated to regulate the voltage at the local bus (B₂). When the absorbed reactive power by the remote DERs was set at values from across the surface provided in Figure 7, such as $Q_{D1} = Q_{D3} = 0.02$ pu for $V_1 = 1$ pu, the voltage at B₂ was almost equal to 1.05 pu, as expected from Equation (7). A slight deviation was observed due to a steady-state error in the injected active and reactive power by the DER at B₂. Figure 8 indicates that if the absorbed reactive power by the remote DERs is assigned over or under the surface, the voltage at the local bus will be lower or higher than 1.05 pu, respectively, which validates the accuracy of the analysis provided in this section.

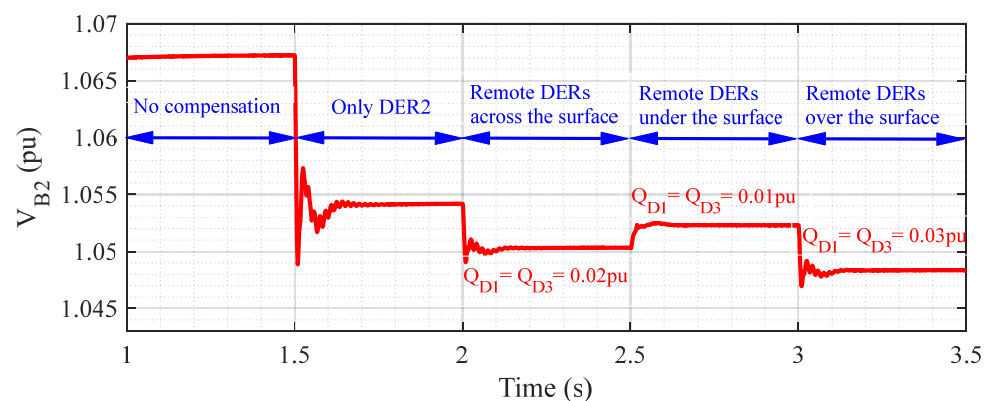


Figure 8. Voltage at B₂ for five different conditions.

3. Description of Proposed Communication System

The proposed communication system topology is based on a distributed level phasor measurement unit (D-PMU or μ PMU) and phasor data concentrator (PDC), as shown in Figure 1. This system leverages the electrical quantities measured by PMUs, which are either used in local controllers or transmitted to the PDC by a central control unit. The updated values of the parameters and/or control commands generated in the PDC are then sent to the local controllers of the DERs. The PMU reports four fundamental measurements in three phases, resulting in a total of 12 measurement channels. These measurements include voltage magnitude, voltage phase angle, current magnitude, and current phase angle per phase, with a maximum sampling rate of 100 and 120 frames per second for a 50 Hz and 60 Hz nominal system frequency, respectively, as recommended by the IEEE C37.118.1 standard. The μ PMU also utilizes a GPS clock to ensure precise time synchronization, which is achieved once the GPS antenna establishes a connection with satellites. This synchronization is achieved by the same-time sampling of voltage and current phasors using timing signals from the GPS receiver. With an accuracy angle of 0.01, a total vector error allowance of 0.05% (precision), an angle resolution of 0.002, and a magnitude resolution of 0.0002%, the μ PMU ensures reliable and accurate measurement. Its accuracy and precision are typically 0.01% and 0.05%, respectively, as per the standard [16].

The PDC is a device designed to receive measurement data packets from the PMUs using a specific protocol, such as TCP/IP packets with the C37.118.2 payload data format. The maximum wait time for a PDC to record phasor measurements from all the PMUs is 14 s. If the phasor data is received within this maximum wait time, the output data is created immediately; otherwise, the PDC waits until the time limit expires to generate the output data. The PDCs aggregate data and send it to downstream consumers in a format defined by IEEE Std. C37.118.2. Communication technologies in PMU-PDC-based systems can be broadly classified into two groups: wired and wireless. Wired communication

technologies offer high reliability, large bandwidth, and protection against interference, while wireless technologies provide advantages such as rapid deployment, low installation and maintenance costs, and access to remote locations [30].

Communication in the proposed algorithm uses wireless technology and can be visualized as a loop that includes PMUs, PDCs, and data transmission, as illustrated in Figure 9. The communication data and channels between the PMUs and the PDC(s) vary based on the stage of operation in the coordination algorithm, which are described below.

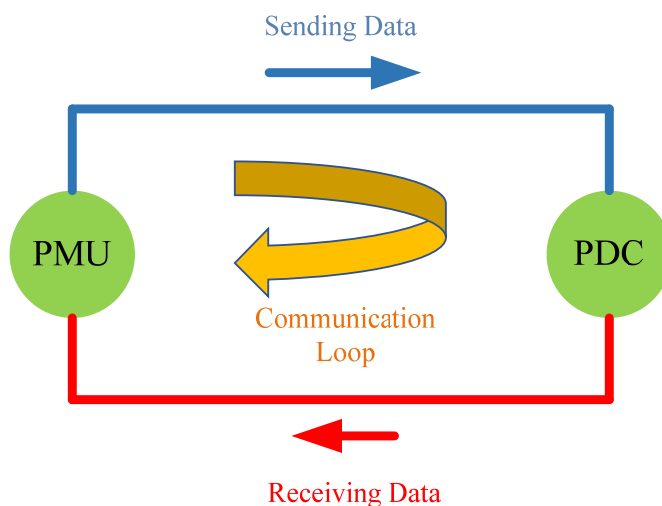


Figure 9. A general view of the proposed communication system.

In Stage I, the PMUs measure and transmit the usual voltage magnitude, voltage phase angle, current magnitude, and current phase angle per phase. In Stage II, the PDC uses the measured voltage magnitude to generate channels with the logical commands 0 (local) or 1 (remote), which includes two channels per PMU. Typically, a maximum of $n - 1$ PMUs are involved in this stage, in a system with n PMUs. Stage III involves 12 channels for measuring the voltage magnitude, voltage phase angle, current magnitude, and current phase angle per phase of all the DERs, and the communication data in this stage include real quantities sent from the PDC and received by all the DERs for updating control parameters. Similarly, in Stage IV, there are 12 channels for voltage and current phasors, as well as an additional channel per DER for the real quantities sent by the PDC and received by the specified local controllers. Table 1 lists the specifications for these stages based on the test system used in this study, which includes three DERs.

Table 1. The specifications for each stage involved in communication.

Stage Number	Sending Data		Receiving Data		Number of Communication Loops
	Maximum Number of PMUs	Data Type	Maximum Number of PMUs	Data Type	
II	2	Voltage and current (Mag. and phase)	2	One-bit binary code	1
III	3	Voltage and current (Mag. and phase)	3	Real quantities	1
IV	2	Voltage and current (Mag. and phase)	2	Real quantities	Maximum 4

4. Evaluating the Results and Discussion

In order to demonstrate the effectiveness of the proposed approach for the coordinated performance of all DERs in voltage regulation, the benchmark IEEE 13-bus radial

distribution feeder (Figure 10) has been modeled in MATLAB. In this system, buses 634, 671, and 675 are assumed as area 1, area 2, and area 3, and selected for connecting DER1, DER2, and DER3, respectively, as illustrated in Figure 10. The performance of the system in terms of the ability of the proposed algorithm to coordinate voltage regulation as well as the accuracy of the communications interface are represented in two separate subsections.

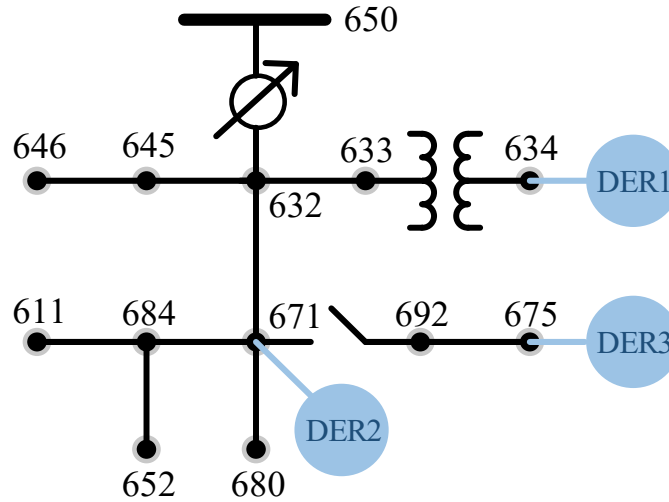


Figure 10. The studied system.

4.1. Ability of the Proposed Algorithm to Coordinate Voltage Control

Three different scenarios have been defined in this subsection to verify the performance and merits of the proposed algorithm.

4.1.1. Scenario 1

In this simulation scenario, an initial voltage increase was applied to the system at $t = 0.4$ s, resulting in voltage level increases in areas 1, 2, and 3 to 1.0655 pu, 1.065 pu, and 1.06 pu, respectively. Figure 11 presents the results of employing the proposed voltage regulation strategy in all three areas. In all the figures in this section, the maximum capability of the DERs in active power and reactive power exchanges is considered as the base value for the generated active power and absorbed reactive power of the DERs, respectively.

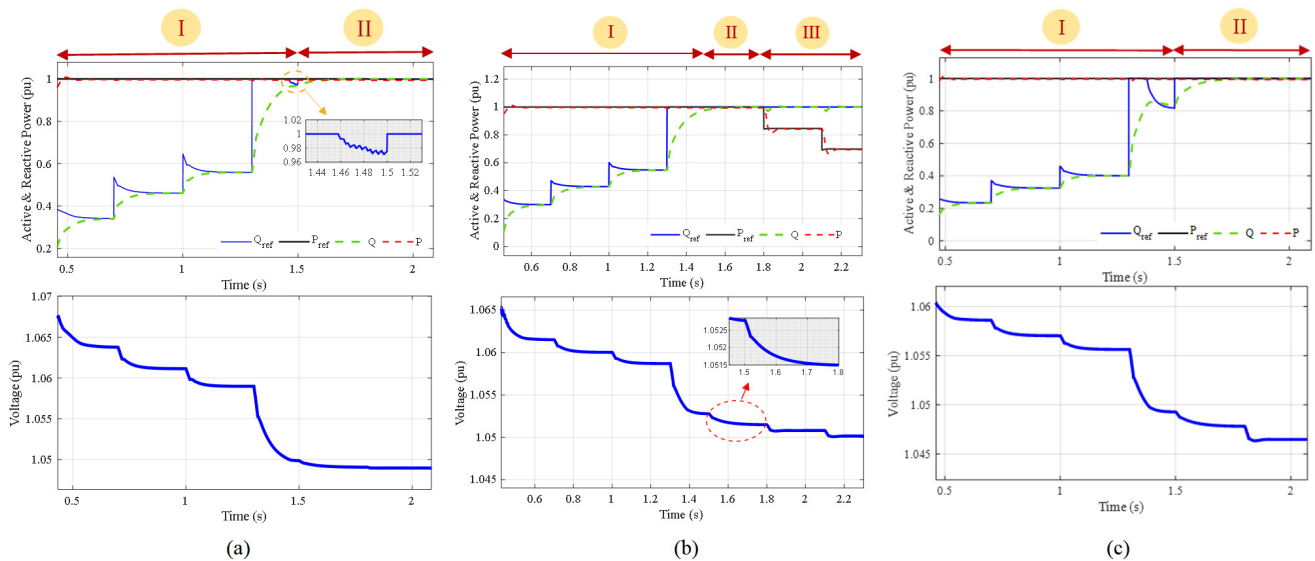


Figure 11. Voltage regulation in all three areas by employing the proposed strategy for scenario 1 in (a) area 1, (b) area 2, and (c) area 3.

Figure 11a,c show that DER1 and DER3 were able to regulate the voltage at the POC in the first stage of the algorithm, as depicted by the flowchart in Figure 4. However, Figure 11b demonstrates that DER2 was not able to control the voltage by locally exchanging reactive power. As a result, the algorithm proceeded to Stage II, and the free capacity of the reactive power of DER1 and DER3 (as depicted by the zoomed-in figures), was utilized. Under this condition, both DER1 and DER3 were listed as remote DERs and set at the maximum value as planned by the central controller. The voltage reduction resulting from the maximum reactive power absorption by DER1 and DER3 is clearly observable in Figure 11a,b. It is notable that all of the capacity of the reactive power resources was utilized before the curtailment occurred in DER2.

Despite the reduction in voltage in DER2 due to the incorporation of other DERs in Stage II, the voltage was not sufficiently reduced to the permitted value of 1.05 pu. Therefore, the algorithm proceeded to Stage III, where the voltage is controlled through local curtailment in area 2 without impacting the other remote DERs in terms of active power curtailment. As seen in Figure 11b, the voltage in area 2 approached 1.05 pu after a 0.3 pu active power curtailment was imposed on DER2 in Stage III. The figure demonstrates that if the voltage in area 2 had not been reduced in Stage II, an additional amount of power curtailment would have been required (without using the proposed algorithm) to restore the voltage to its prescribed level of 1.05 pu.

To assess the effectiveness of the proposed strategy and demonstrate its practical benefits over non-coordinated methods, the same test was repeated without implementing the proposed algorithm. Figure 12 shows the active and reactive power in all the DERs, as well as the voltage at the connection points. According to Figure 12a,c, the voltage in areas 1 and 3 were restored locally by absorbing reactive power at DER1 and DER3 within 1.1 s and less than 1 s, respectively. The results for area 2, depicted in Figure 12b, indicate that even with the maximum reactive power absorption and a minimum generation level of 0.2 pu (maximum curtailment) in DER2, the voltage could not be recovered. By comparing Figures 11 and 12, it becomes evident how the proposed coordinated approach helps to regulate the voltage in area 2. By incorporating DER1 and DER3 in absorbing reactive power at $t = 1.5$ s in Stage II of the algorithm, the voltage in area 2 was restored after only a 30% curtailment of DER2. The responses of the voltages in the three areas during this scenario are given in Figure 13, as compared to the case when only a local control is used (without coordination), which further illustrates the impact of the remote DERs in the proposed coordinated algorithm to regulate the voltage.

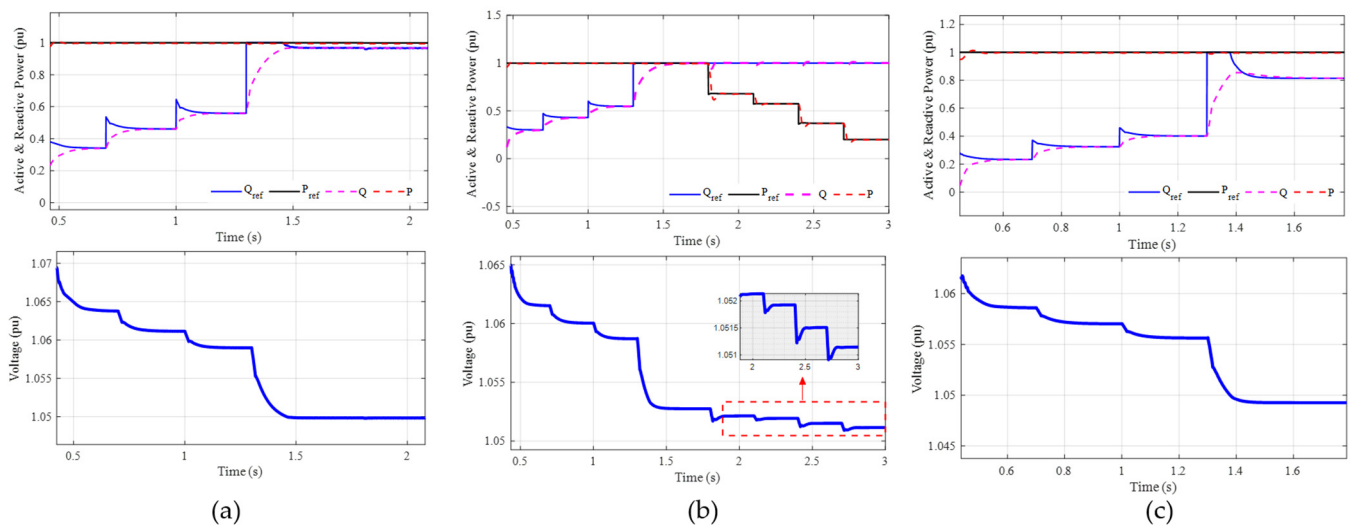


Figure 12. Voltage regulation in all three areas for scenario 1 with no coordination strategy in (a) area 1, (b) area 2, and (c) area 3.

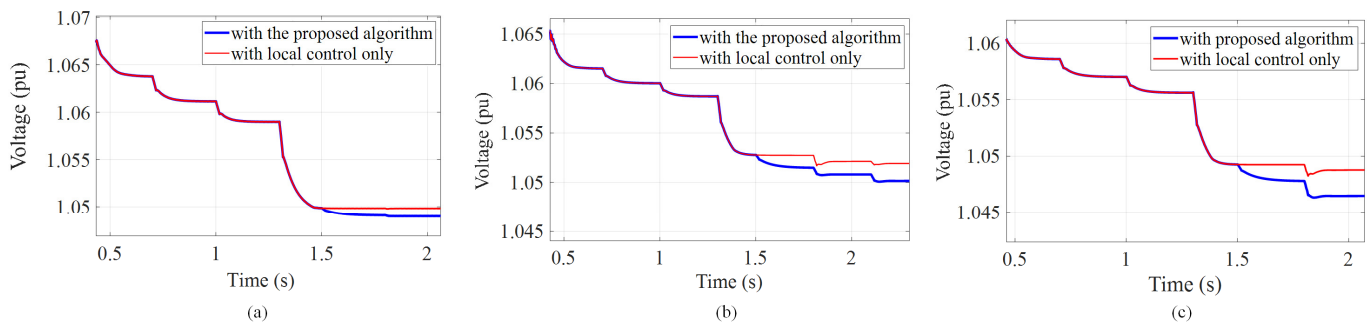


Figure 13. Comparison of the voltage response of the proposed coordinated approach with a local control only in (a) area 1, (b) area 2, and (c) area 3.

4.1.2. Scenario 2

This scenario aims to investigate the effectiveness of the supplementary condition implemented in Stage III of the proposed algorithm for improving active power curtailment in the system, as shown in Figure 4 and explained in Section 2.2. An increased voltage occurs at $t = 0.4$ s in this scenario. Figure 14 shows the active and reactive power in all three areas, as well as the voltage at the connection points when the supplementary loop is not employed in Stage III. As shown in Figure 14a, the voltage in area 1 was restored within 1.6 s after passing through three stages and imposing a 0.3 pu curtailment of DER1. In Figure 14b, it can be seen that the voltage in area 2 was controlled in Stage III within 2.2 s with a 60% curtailment of DER2. The voltage in area 3 was recovered in the first stage after less than 1 s, as depicted in Figure 14c. The impact of the central control unit in voltage regulation is highlighted in the zoomed-in Figure 14b. The curtailment index (CI) and the curtailment dispatch (CD) were calculated to be 0.3 and 0.1, respectively, based on equations (1) and (2). The system voltage in all areas was restored after 2.2 s.

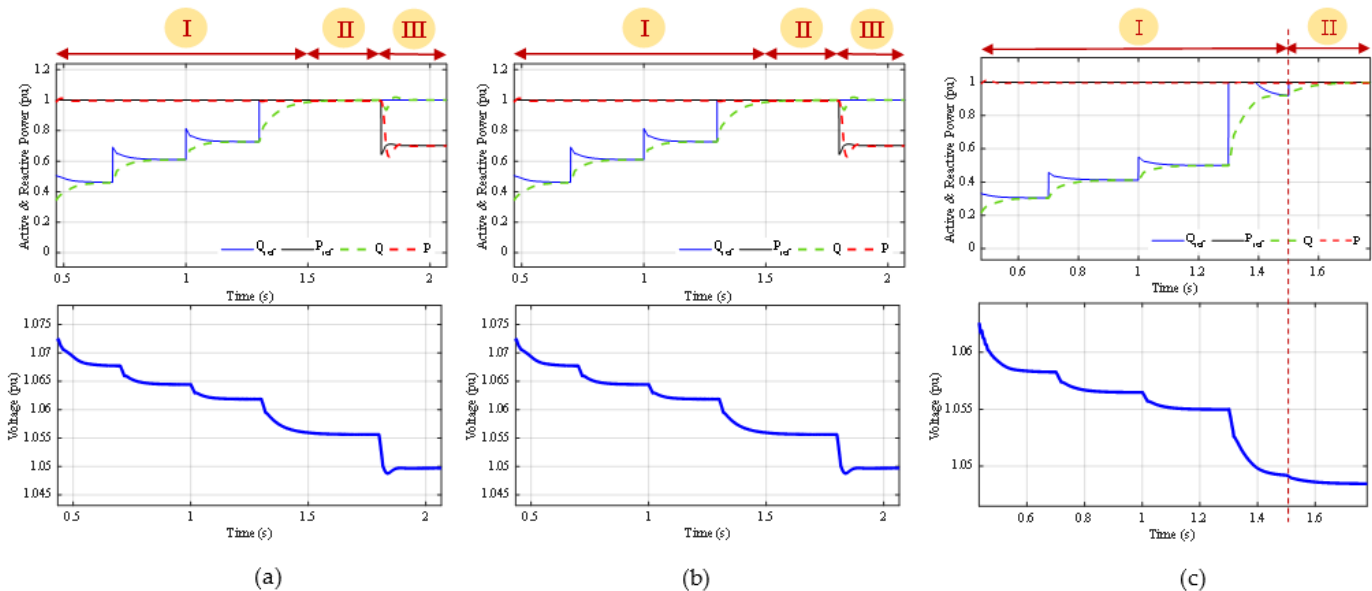


Figure 14. Voltage regulation in all three areas for scenario 2 with no supplementary loop in the Stage III strategy in (a) area 1, (b) area 2, and (c) area 3. The red vertical line highlights some significant transition times from a stage to another.

Figure 15 demonstrates the impact of incorporating the supplementary loop in Stage III. As shown in Figure 15b,c, the voltage in area 2 was restored within 1.6 s by making 0.258 pu curtailments in DER3 at $t = 1.8$ s, while suffering only a 0.3 pu curtailment of DER2. This approach results in a decrease in the curtailment index (CI) and the curtailment dispatch (CD) to 0.186 and 0.062, respectively, and a reduction in the recovery time to 1.6 s.

By rescheduling in the central controller before the algorithm finishes in Stage 3, not only is the recovery time decreased, but curtailment is also dispatched more equitably across the system with a lesser amount of CI.

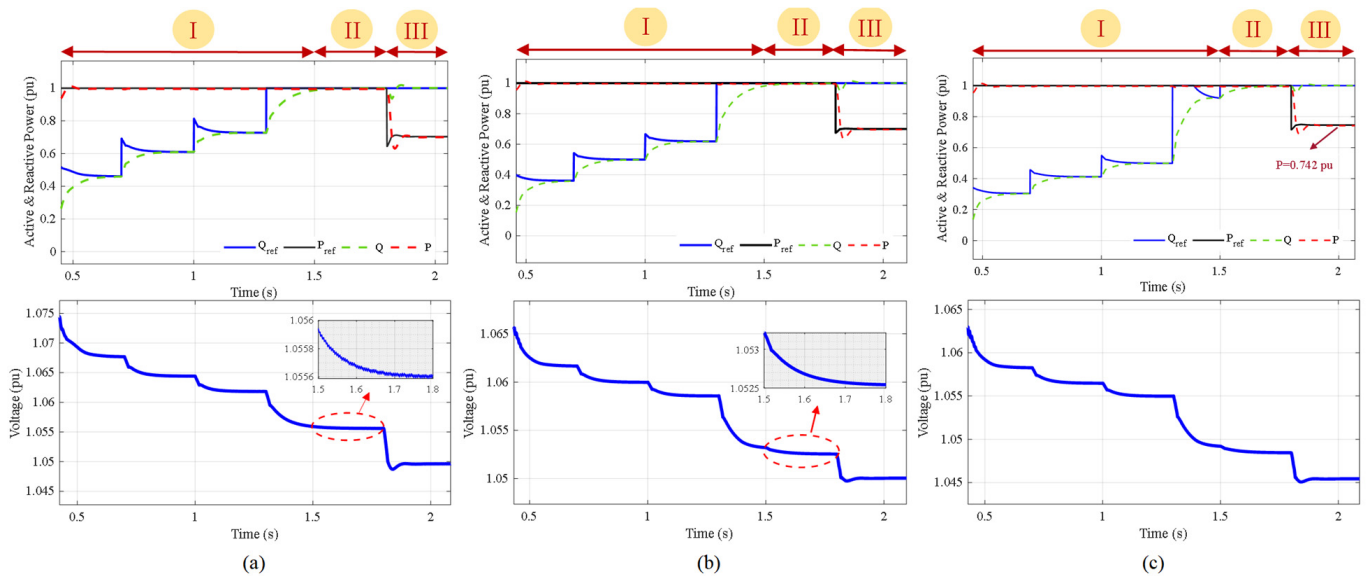


Figure 15. Voltage regulation in all three areas when the supplementary-loop strategy in Stage III is employed in (a) area 1, (b) area 2, and (c) area 3.

4.1.3. Scenario 3

The previous tests evaluated the system under conditions where all three areas experienced similar voltage increases, and all the DERs initially regulated the voltage at the POC through local controllers in Stage I. The remaining reactive power exchange capacity was utilized in Stage II to reduce the voltage rise before any curtailment occurred. This scenario, however, examines a situation where one area does not experience a voltage increase, but absorbs the maximum reactive power in Stage II to regulate the system voltage in the other areas. Figure 16 presents the results of this scenario, including the active and reactive power in all three areas, as well as the voltage at the connection points. As shown in the figure, only areas 2 and 3 experienced a voltage increase, and the voltage in area 1 remained within the permissible range. DER2 was able to regulate the voltage in area 2 at $t = 1.3$ s after passing through Stage I, as depicted in Figure 16b. In Figure 16c, it can be observed that the voltage in area 3 was not restored in Stage I, so the algorithm proceeded to Stage II, where DER1 absorbed its maximum exchangeable capacity, as shown in Figure 16a. As a result of absorbing reactive power in area 1, the voltage in area 3 decreased, as demonstrated in the zoomed-in figure. The system voltage was ultimately restored in Stage III, following a 0.5 pu curtailment of DER3 at $t = 2.4$ s. It is worth noting that the voltage in area 1 did not drop below the lower permissible limit (0.95 pu). However, in other systems with different power flows and specifications, the voltage may fall below the limit, which can be problematic. To address this issue, supplementary loops are included in Stages II and IV to exclude any potential effect on the DERs, as described in Section 2.

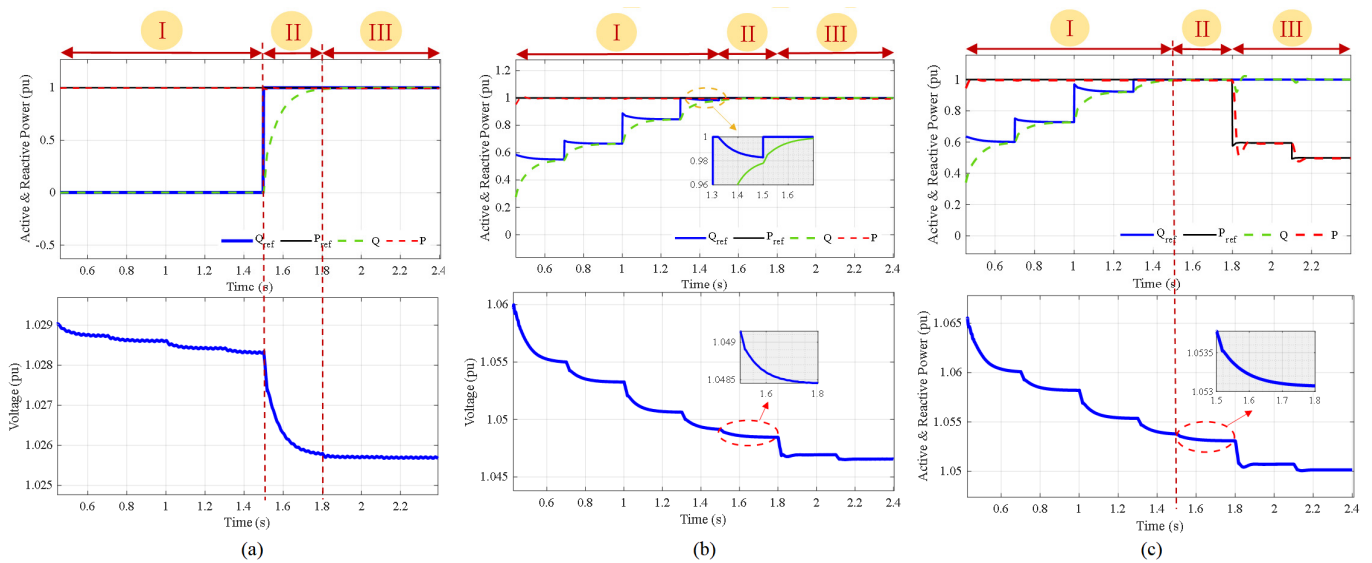


Figure 16. Voltage regulation in all three areas for scenario 3 when two DERs suffer from the increased voltage strategy in (a) area1, (b) area 2, (c) area 3. The red vertical line highlights some significant transition times from a stage to another.

4.2. Application of the Algorithm on a Larger Test System

In the previous section, a comprehensive examination of the proposed coordinated control strategy was conducted on a small-scale test system to establish its efficacy through a detailed analysis. To further evaluate its scalability, the performance of the coordinated control strategy was assessed on the IEEE 33-bus Benchmark system [31], serving as the second studied system. A single diagram of the network is presented in Figure 17.

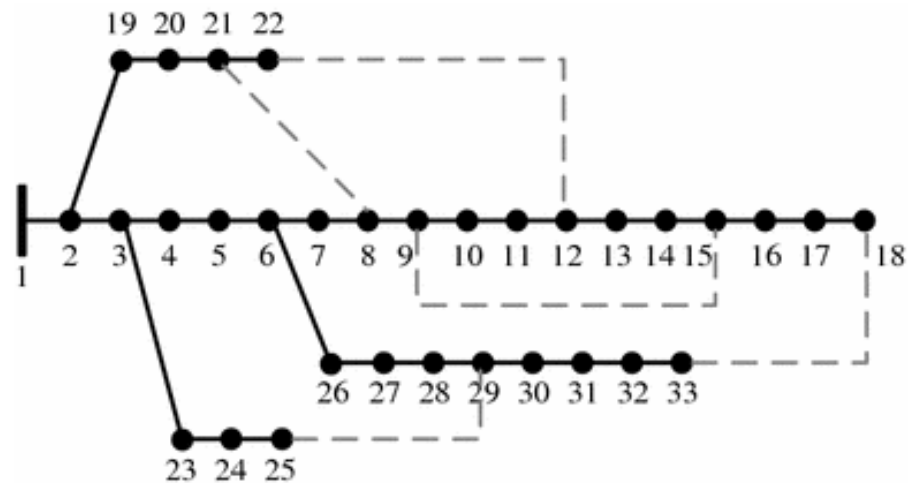


Figure 17. A single line diagram of the IEEE 33-bus system.

According to Figure 17, buses 6, 18, 21, 25, and 33 are assigned as the points of connection (POC) for five DERs. The voltage at B6, B18, B21, B25, and B33 are assumed to be increased to 1.0582, 1.584, 1.0649, 1.0537, and 1.0575, respectively. The DER connected to B21 is considered local, and the others are assumed to be remote buses. Figure 18 shows how reactive power absorption at the local DER has an impact on the remote ones.

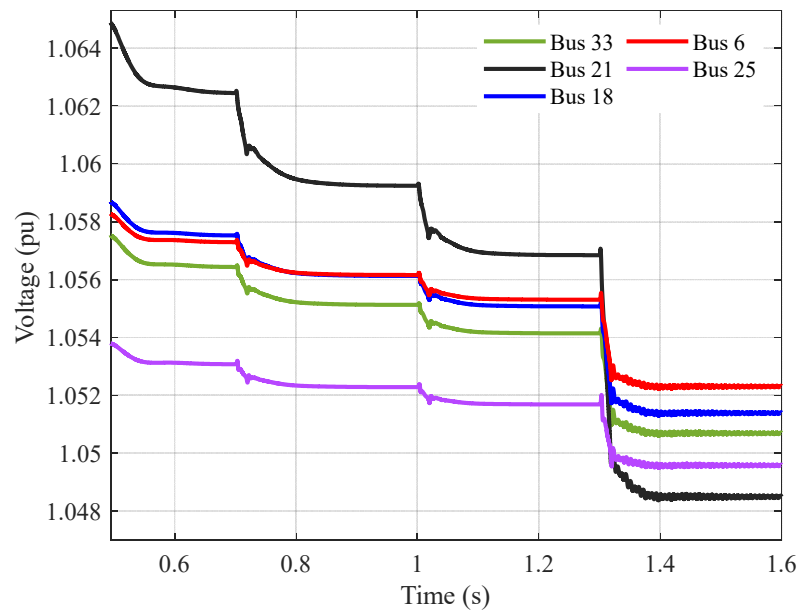


Figure 18. Voltage response of the selected DERs at the IEEE 33-bus system.

According to the figure, the local controller not only reduces the voltage at B21 to below 1.05 as the target value, but also is able to reduce the voltage at B6, B18, B25, and B33 to 1.0522, 1.513, 1.0495 (lower than 1.05), and 1.0507, respectively. The reactive power absorbed by the local DER and the reference value are illustrated in Figure 19. It is visible from the figure that the DER is able to follow the reference value accurately with no transient distortion or steady-state error. This test demonstrates that the proposed control system is able to be employed in systems with more buses and different configurations.

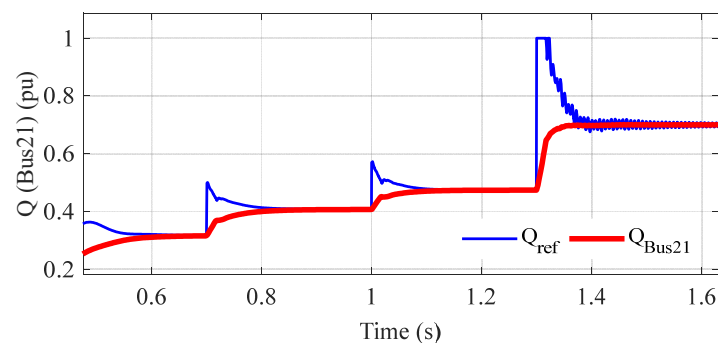


Figure 19. The reactive power absorbed by the local DER and the reference value.

It should be noted that, while there is no strict limit on the number of DERs that can be employed in the proposed algorithm, in practice, the limit depends on the capacity of the PDC to handle multiple PMUs. In general, the number of PMUs that can be connected to one PDC depends on its processing power, memory, and communication bandwidth. A PDC needs to efficiently manage the incoming data streams from multiple PMUs, process and analyze the phasor measurements, and store or transmit the data to the appropriate applications or control centers. Therefore, the capability of the PDC to handle a large number of PMUs may be limited by its technical specifications and processing capabilities.

4.3. Accuracy of the Communication System

The performance of the communication between the PMU and PDC is evaluated using the specifications for LTE (4G) technology. Each resource block is 0.5 ms long and a path loss exponent of three is considered. The path loss is modeled as $(d/d_0)^3$, where d is the

actual distance between the PMU and PDC and d_0 is the reference distance. The channel gain is inversely proportional to this path loss. The communication model considers a 4-QAM modulation. The accuracy of the communication system in the proposed algorithm is discussed in the following subsection in terms of the influence of the noise and the impact of the communication delay.

4.3.1. Influence of the Noise

The accuracy of the communication system is affected by the signal-to-noise ratio (SNR). When the SNR is low, there are an increasing number of samples which are incorrectly received, leading to potential errors in the received measurements. In this study, the impact of SNR on the accuracy of the communication system is investigated using monitoring data transmission from the PMU to PDC. Figure 20a–d show the voltage and current magnitude, as well as the voltage and current phase angles, respectively, for a certain instance of monitoring data transmission from the PMU to PDC when the SNR is 10 dB. On the other hand, Figure 21a–d show the voltage and current magnitude, and the voltage and current phase angles, respectively, for 0 dB SNR. The comparison between these two scenarios provides valuable insights into the effects of low SNR on the received measurements. It can be clearly observed that when the SNR is low, there are an increasing number of samples which are incorrectly received, with an error level of up to 30% in the voltage magnitude and 200% in the voltage phase angle. Since this paper is concerned with voltage regulations, errors in the voltage magnitudes could potentially impact the performance of the algorithm employed in this study.

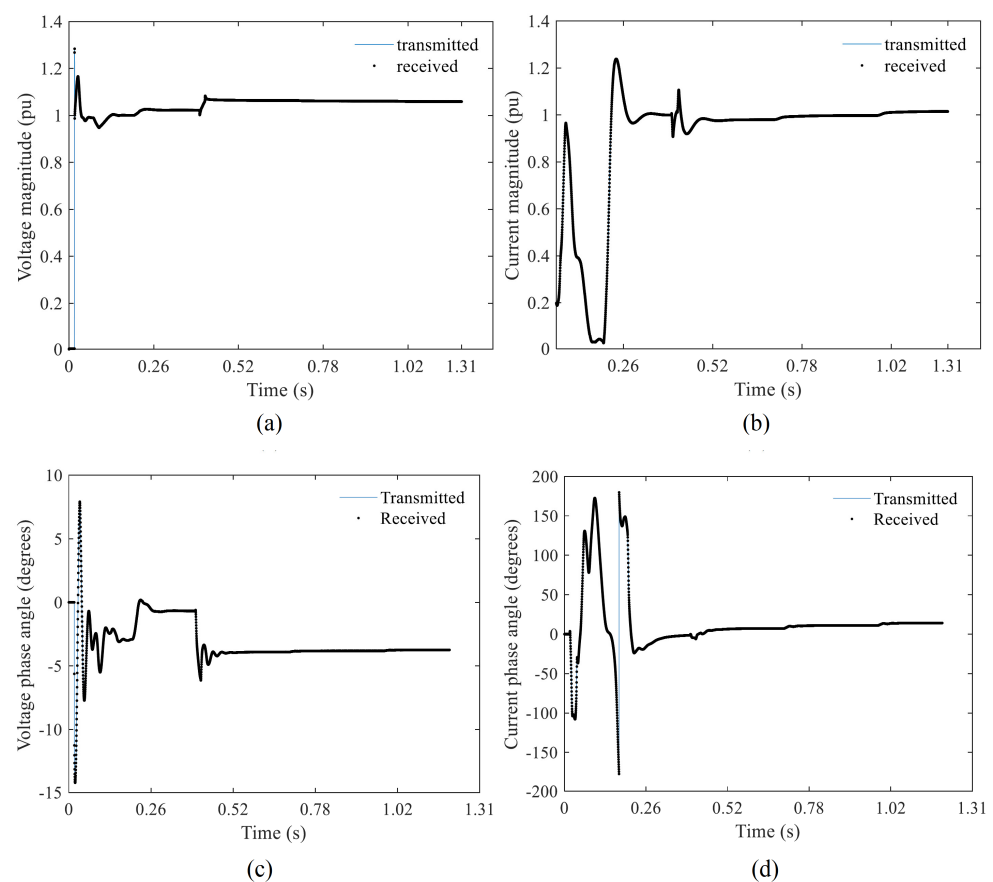


Figure 20. Transmitted and received voltage and current magnitudes (a,b) and phase angles (c,d) through the communication channel between the PMU and PDC with SNR = 10 dB.

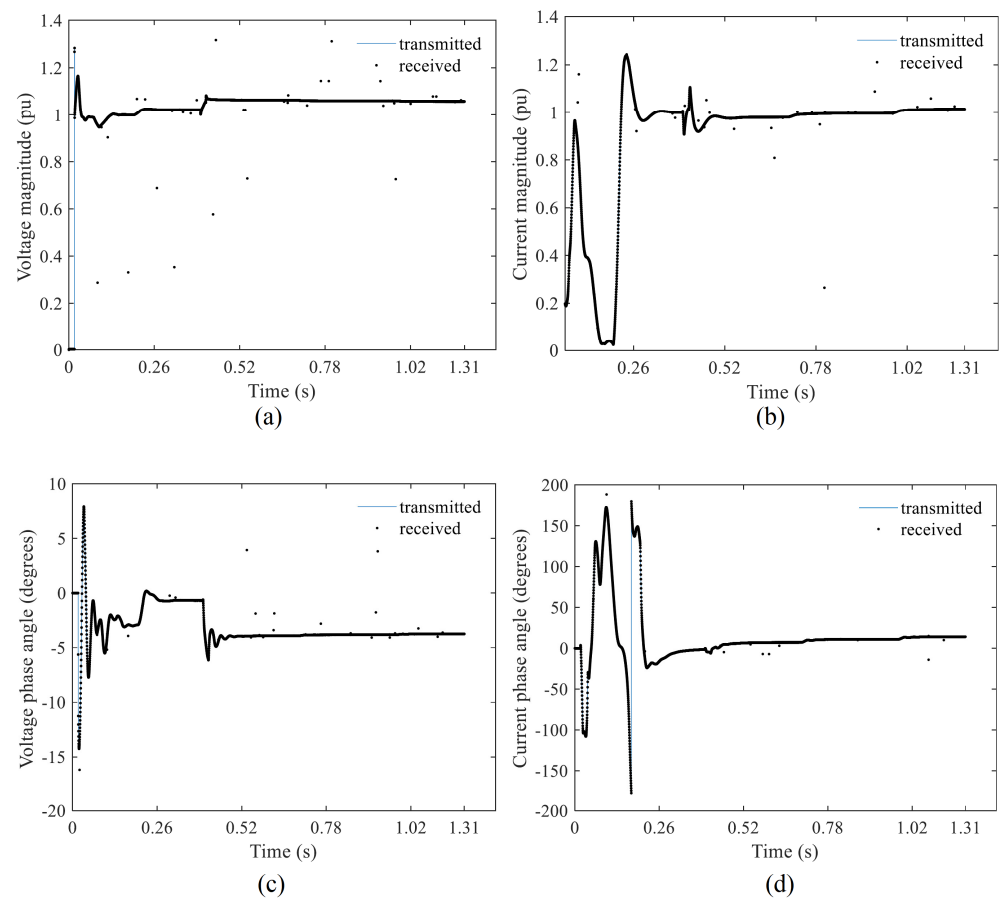


Figure 21. Transmitted and received voltage and current magnitudes (a,b) and phase angles (c,d) through the communication channel between the PMU and PDC with SNR = 0 dB.

In particular, the impact of voltage magnitude errors primarily affects Stage II of the algorithm. In this stage, the algorithm relies on accurate voltage measurements to make decisions regarding the inclusion or exclusion of DERs. If a DER's reported voltage is mistakenly received as a very low voltage level, it may be erroneously excluded from the voltage regulation process. Conversely, if a DER's reported voltage is mistakenly received as a high voltage level, it may be mistakenly included as a remote DER. However, it is important to note that if the actual voltage level at those DERs decrease due to reactive power absorption, the local control of those DERs will initiate voltage regulation to mitigate any potential issues.

4.3.2. Impact of Communication Delay

Figure 22 shows the communication delay between the PMU and PDC for (a) different channel gains (10 dB SNR) and (b) different noise power levels (channel gain 20) between the PMU and PDC. It can be observed that the communication delay varies between 0.5 ms and 2 ms (given that the LTE resource blocks have a discrete length). When the channel gain is high, most of the samples are transmitted within a 1.5 ms communication delay, which is not true when the channel gain is low. Similar observations can be made for different noise power levels. With an increasing SNR, more samples can be transmitted with a smaller delay.

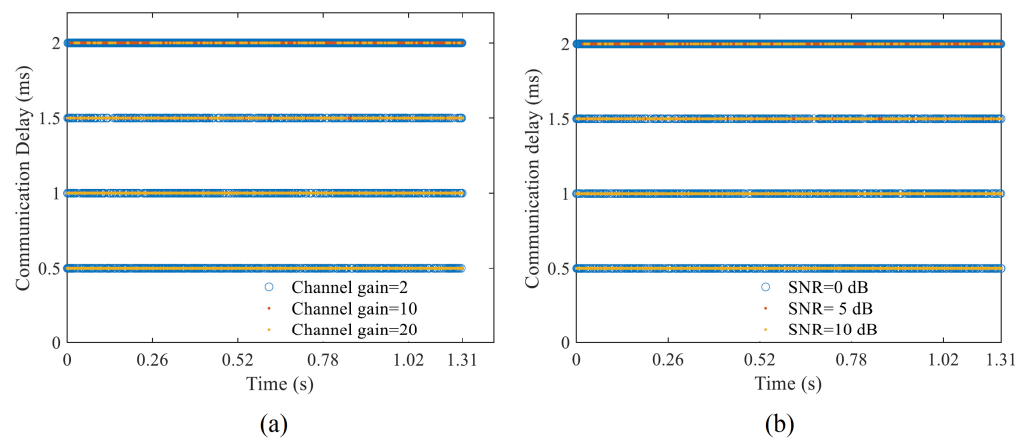


Figure 22. Communication delay between the PMU and PDC for (a) different channel gains and (b) different noise power levels.

Figure 23 shows the communication error rates for transmission between the PMU and PDC for (a) different channel gains (10 dB SNR) and (b) different noise power levels (channel gain 20). It can be observed that for a lower channel gain, the probability of receiving incorrect samples becomes higher. With a 10-fold increase in channel gain, this probability can be decreased by more than 10-fold. Similarly, for an increasing SNR, a smaller error probability can be observed.

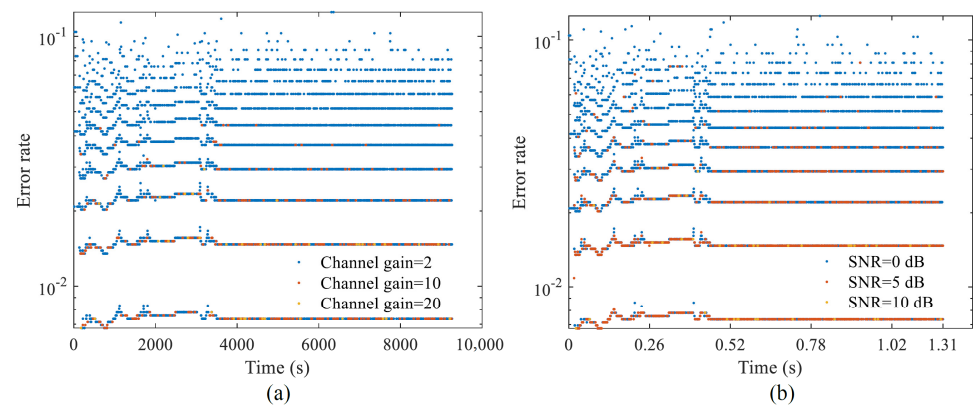


Figure 23. Error rate for communication between the PMU and PDC for (a) different channel gains and (b) different noise power levels.

It is pertinent to highlight that the failure of the communication system will not impact the operation of the DERs, as they will regulate the voltage locally in the traditional way. The coordination algorithm is added as an additional layer which ensures the efficient restoration of the voltage with minimum power curtailment.

5. Conclusions

The hierarchical multi-stage algorithm proposed in this study has demonstrated its effectiveness in achieving coordinated voltage control in distribution systems. The algorithm, which consists of four stages, employs a combination of reactive power absorption and power generation curtailment to restore the system voltage, with communication based on the PMU at the local controllers and the PDC at the central control unit facilitating data exchange between the DERs and the central controller. By prioritizing reactive power absorption over curtailment, the proposed algorithm reduces unnecessary curtailment, leading to a more efficient voltage control system based on PMU-PDC communication technology. The simulation results obtained using the IEEE 13-bus radial distribution benchmark system confirmed the efficacy of the proposed control system for achieving

coordinated voltage control and ensuring the accuracy of the PMU-PDC communication interface. In addition, to demonstrate its scalability, the proposed coordinated algorithm was successfully applied to the IEEE 33-bus distribution network, showcasing its effectiveness across a larger system. Overall, the proposed hierarchical control strategy based on PMU-PDC provides an effective means for improving voltage control in distribution systems and represents a promising area for future research.

Author Contributions: Conceptualization, A.Z., A.G., N.H. and M.A.; methodology, A.Z., A.G. and S.I.; software, A.Z.; validation, A.Z., A.G. and N.H.; formal analysis, all authors; investigation, all authors; resources, all authors; writing—original draft preparation, A.Z. and A.G.; writing—review and editing, all authors; visualization, all authors; project administration, A.G. and M.A. All authors have read and agreed to the published version of the manuscript.

Funding: This work was funded by Deakin University under the 2022 Mini ARC Analog Program—Linkage (PJ02540).

Data Availability Statement: For more information, please contact the research group at: <https://www.deakin.edu.au/engineering/research/centre-for-smart-power-and-energy-research>.

Conflicts of Interest: The authors declare no conflict of interest.

References

1. ANSIC84.1-2016; American National Standard for Electric Power Systems and Equipment—Voltage Ratings (60 Hz). ANSI: Rosslyn, VA, USA, 2016.
2. IEEE Std 1547-2018 (Revision of IEEE Std 1547-2003); IEEE Standard for Interconnection and Interoperability of Distributed Energy Resources with Associated Electric Power Systems Interfaces—Redline. IEEE: New York, NY, USA, 2018; pp. 1–227.
3. Afandi, I.; Agalgaonkar, A.P.; Perera, S. Integrated Volt/Var Control Method for Voltage Regulation and Voltage Unbalance Reduction in Active Distribution Networks. *Energies* **2022**, *15*, 2225. [[CrossRef](#)]
4. Wang, X.; Wang, L.; Kang, W.; Li, T.; Zhou, H.; Hu, X.; Sun, K. Distributed Nodal Voltage Regulation Method for Low-Voltage Distribution Networks by Sharing PV System Reactive Power. *Energies* **2023**, *16*, 357. [[CrossRef](#)]
5. Tang, Z.; Hill, D.J.; Liu, T. Distributed Coordinated Reactive Power Control for Voltage Regulation in Distribution Networks. *IEEE Trans. Smart Grid* **2021**, *12*, 312–323. [[CrossRef](#)]
6. Tewari, T.; Mohapatra, A.; Anand, S. Coordinated Control of OLTC and Energy Storage for Voltage Regulation in Distribution Network with High PV Penetration. *IEEE Trans. Sustain. Energy* **2021**, *12*, 262–272. [[CrossRef](#)]
7. Guo, Y.; Wu, Q.; Gao, H.; Chen, X.; Østergaard, J.; Xin, H. MPC-Based Coordinated Voltage Regulation for Distribution Networks with Distributed Generation and Energy Storage System. *IEEE Trans. Sustain. Energy* **2019**, *10*, 1731–1739. [[CrossRef](#)]
8. Suresh, A.; Bisht, R.; Kamalasadana, S. A Coordinated Control Architecture with Inverter Based Resources and Legacy Controllers of Power Distribution System for Voltage Profile Balance. *IEEE Trans. Ind. Appl.* **2022**, *58*, 6701–6712. [[CrossRef](#)]
9. Mehmood, K.K.; Khan, S.U.; Lee, S.J.; Haider, Z.M.; Rafique, M.K.; Kim, C.H. A real-time optimal coordination scheme for the voltage regulation of a distribution network including an OLTC, capacitor banks, and multiple distributed energy resources. *Int. J. Electr. Power Energy Syst.* **2018**, *94*, 1–14. [[CrossRef](#)]
10. Bedawy, A.; Yorino, N.; Mahmoud, K.; Lehtonen, M. An Effective Coordination Strategy for Voltage Regulation in Distribution System Containing High Intermittent Photovoltaic Penetrations. *IEEE Access* **2021**, *9*, 117404–117414. [[CrossRef](#)]
11. Xu, R.; Zhang, C.; Xu, Y.; Dong, Z.; Zhang, R. Multi-Objective Hierarchically-Coordinated Volt/Var Control for Active Distribution Networks with Droop-Controlled PV Inverters. *IEEE Trans. Smart Grid* **2022**, *13*, 998–1011. [[CrossRef](#)]
12. Zhang, Z.; Dou, C.; Yue, D.; Zhang, Y.; Zhang, B.; Li, B. Regional Coordinated Voltage Regulation in Active Distribution Networks with PV-BESS. *IEEE Trans. Circuits Syst. II: Express Briefs* **2022**, *70*, 596–600. [[CrossRef](#)]
13. Long, Y.; Elliott, R.T.; Kirschen, D.S. Adaptive Coalition Formation-Based Coordinated Voltage Regulation in Distribution Networks. *IEEE Trans. Power Syst.* **2022**, *37*, 2005–2018. [[CrossRef](#)]
14. Hu, X.; Liu, Z.-W.; Wen, G.; Yu, X.; Liu, C. Voltage Control for Distribution Networks via Coordinated Regulation of Active and Reactive Power of DGs. *IEEE Trans. Smart Grid* **2020**, *11*, 4017–4031. [[CrossRef](#)]
15. Nazari-pouya, H.; Pota, H.R.; Chu, C.-C.; Gadh, R. Real-Time Model-Free Coordination of Active and Reactive Powers of Distributed Energy Resources to Improve Voltage Regulation in Distribution Systems. *IEEE Trans. Sustain. Energy* **2020**, *11*, 1483–1494. [[CrossRef](#)]
16. Dusabimana, E.; Yoon, S.-G. A Survey on the Micro-Phasor Measurement Unit in Distribution Networks. *Electronics* **2020**, *9*, 305. [[CrossRef](#)]
17. Dong, Q.; Sun, J.; Wu, Q.; Liu, Y. A Method for Filtering Low Frequency Disturbance in PMU Data before Coordinated Usage in SCADA. *IEEE Trans. Power Syst.* **2017**, *32*, 2810–2816. [[CrossRef](#)]

18. Blas, L.L.F.; Bundoc, P.E.D.C.; Melchor, K.C.L.; Orillaza, J.R.C. Micro-Synchrophasors for Event Detection in an Electric Power System Simulator. In Proceedings of the IEEE Innovative Smart Grid Technologies—Asia (ISGT Asia), Singapore, 22–25 May 2018; pp. 178–183.
19. Sun, Y.; Chen, X.; Yang, S.; Tseng, K.J.; Amaratunga, G. Micro PMU Based Monitoring System for Active Distribution Networks. In Proceedings of the IEEE 12th International Conference on Power Electronics and Drive Systems (PEDS), Honolulu, HI, USA, 12–15 December 2017; pp. 518–522.
20. *IEEE Std C37.118.1-2011 (Revision of IEEE Std C37.118-2005)*; IEEE Standard for Synchrophasor Measurements for Power Systems. IEEE: New York, NY, USA, 2011; pp. 1–61.
21. Stewart, E.; Liao, A.; Roberts, C. *Open mPMU: A Real World Reference Distribution Micro-Phasor Measurement Unit Data Set for Research and Application Development*; Technical Report 1006408; LBNL: Berkeley, CA, USA, 2016.
22. Gargoom, A.; Elmusrati, M.; Gaouda, A. Enhancing the operation of smart inverters with PMU and data concentrators. *Int. J. Electr. Power Energy Syst.* **2022**, *140*, 108077. [[CrossRef](#)]
23. Von Meier, A.; Culler, D.; McEachern, A.; Arghandeh, R. *Micro-Synchrophasors for Distribution Systems*; ISGT: Washington, DC, USA, 2014; pp. 1–5.
24. Arghandeh, R. Micro-Synchrophasors for Power Distribution Monitoring, a Technology Review, systems and Control. *arXiv* **2016**, arXiv:1605.02813.
25. Von Meier, A.; Stewart, E.; McEachern, A.; Andersen, M.; Mehrmanesh, L. Precision Micro-Synchrophasors for Distribution Systems: A Summary of Applications. *IEEE Trans. Smart Grid* **2017**, *8*, 2926–2936. [[CrossRef](#)]
26. Liu, Y.; Wu, L.; Li, J. D-PMU based applications for emerging active distribution systems: A review. *Electr. Power Syst. Res.* **2020**, *179*, 106063. [[CrossRef](#)]
27. Eto, J.H.; Stewart, E.M.; Smith, T.; Buckner, M.; Kirkham, H.; Tuffner, F.; Schoenwald, D.A. *Scoping Study on Research and Development Priorities for Distribution-System Phasor Measurement Units*; Lawrence Berkeley National Laboratory: Berkeley, CA, USA, 2015.
28. *IEEE PC37.118.2/D3.2*; IEEE Draft Standard for Synchrophasor Data Transfer for Power Systems. IEEE: New York, NY, USA, 2011; pp. 1–54.
29. Kersting, W.H. Radial distribution test feeders. *IEEE Trans. Power Syst.* **1991**, *6*, 975–985. [[CrossRef](#)]
30. Zurawski, R. From Wireline to Wireless Networks and Technologies. *IEEE Trans. Ind. Inform.* **2007**, *3*, 93–94. [[CrossRef](#)]
31. Dolatabadi, S.H.; Ghorbanian, M.; Siano, P.; Hatziargyriou, N.D. An Enhanced IEEE 33 Bus Benchmark Test System for Distribution System Studies. *IEEE Trans. Power Syst.* **2021**, *36*, 2565–2572. [[CrossRef](#)]

Disclaimer/Publisher’s Note: The statements, opinions and data contained in all publications are solely those of the individual author(s) and contributor(s) and not of MDPI and/or the editor(s). MDPI and/or the editor(s) disclaim responsibility for any injury to people or property resulting from any ideas, methods, instructions or products referred to in the content.